Accepted for publication in Earth Surface Processes and Landforms (9th September 2019)

Google Earth as a data source for investigating river forms and processes: Discriminating river types using form-based process indicators

Alexander J. Henshaw[1*], Prima W. Sekarsari[1,2], Guido Zolezzi[2] and Angela M. Gurnell[1]

[1] School of Geography, Queen Mary University of London, London, UK

[2] Department of Civil, Environmental and Mechanical Engineering, University of Trento, Trento, Italy

* Corresponding author: Alex Henshaw, School of Geography, Queen Mary University of London, Mile End Road, London, E1 4NS, UK; a.henshaw@qmul.ac.uk; +44 (0)207 882 5436

ABSTRACT

Google Earth provides potential for exploiting an enormous reservoir of freely-available remotely sensed data to support river science and management. In this paper, we consider how the platform can support investigation of river physical forms and processes by developing an empirically-based reach-scale classification of semi-natural European single thread to transitional rivers. Using strict reach and image selection criteria, we identified 194 reaches of 68 rivers for analysis. Measurements of channel dimensions and counts of in-channel and floodplain features, standardised for reach length and channel width where necessary, were used to derive a series of geomorphologically-relevant process indicators. A suite of multivariate analyses were then applied to this data set, resulting in the discrimination of five river types: laterally

stable, laterally active sinuous-meandering; transitional (near-braided); bedrock; and cascade/step dominated. The results of the classification were tested by examining the characteristics and distribution of the river classes in relation to known independent controls of river form including reach-scale energy and valley confinement conditions. Our results show that if methods of data extraction are carefully developed, physically meaningful river reach discrimination can be achieved using Google Earth. Although there are limits to the types of information that can be extracted such that field investigations cannot always be avoided, there is enormous potential to mine Google Earth across different space and time scales, supporting the assembly of large, reliable data sets relevant to river forms and processes in a very cost-effective way.

KEYWORDS

Google Earth, form, process, geomorphic units, river classification

INTRODUCTION

Google Earth as a potential information source for investigating river forms and processes

Bizzi et al. (2015) and Marcus and Fonstad (2010) reviewed the many possibilities for supporting research relevant to river science and management that are offered by advances in remote sensing technologies and data analysis techniques, and the increasing availability of remotely sensed data sets. They concluded that data acquisition costs remain relatively high and data processing usually requires significant expertise, with the result that the use of remote sensing data in river science continues to be focused on resolving specific questions and developing sophisticated modelling methodologies (e.g. Alber and Piégay, 2011; Schmitt et al., 2014), usually in relation to particular geographical areas of interest. However, Google Earth is highlighted as a freely available global information system that provides a range of remotely-sensed data sets in a format that can be easily used by river scientists and practitioners who have little background in remote sensing. Thus, Google Earth provides some potential for exploiting remotely sensed data more widely within river science and management (e.g. Large and Gilvear, 2015).

Google Earth incorporates a virtual globe based on the World Geodetic System 1984 (WGS 1984) onto which geographical information is projected. Data layers include satellite and aerial images which are georeferenced to the same virtual globe. The typical baseline resolution of Google Earth data varies across the Earth's surface according to the imagery incorporated within the information system. Across Europe, the study area for the research reported herein, recent images are often of high spatial resolution because of the wide availability of airborne imagery with resolutions of 0.15-

0.30 m. Where imagery is acquired by satellite, the resolution varies from approximately 0.3-0.5 m (Digital Globe's WorldView platform) to 10-30 m (ESA's Sentinel 2 and NASA's Landsat 8). Historical imagery (usually extending back to ca. 2000, but sometimes to the mid-twentieth century) is also available for most locations. In addition, digital elevation data from NASA's Shuttle Radar Topography Mission (SRTM, Farr et al., 2007) are incorporated into Google Earth and the data can be extracted as point elevations. Google Earth therefore represents a potentially significant source of information to support many environmental investigations because it is freely available, it integrates a vast selection of images as well as digital elevation data, and it provides tools to extract elevation and distance measurements.

Morphological classification of rivers

The physical attributes (i.e. size, shape, bed and bank materials, constituent geomorphic/habitat features) and behavioural characteristics (i.e. magnitude, frequency and style of adjustment, sensitivity) of rivers are determined by controls that operate over a range of spatial and temporal scales (Brierley and Fryirs, 2005). For example, lithology and tectonic setting influence both the potential energy available to a river to perform geomorphic work (via their effect on elevation, slope and valley width) and the amount and type of sediment available for transport. Likewise, climate (both directly and indirectly through its control on vegetation) influences the magnitude, frequency and sequencing of flow and sediment transport. Spatial variation in these boundary conditions along and between rivers gives rise to different process interactions that combine to produce remarkable reach-scale diversity in terms of river appearance and responses to individual flood events.

This fundamental link between form and process has provided the theoretical basis upon which numerous river classification schemes have been developed (e.g. Schumm, 1977; Montgomery and Buffington, 1997; Brierley and Fryirs, 2005; Beechie et al., 2006; Gurnell et al., 2016). Such classifications share a common goal of seeking to simplify the complexity of natural landscapes by identifying locations that function in similar ways (Tadaki et al., 2014; Kondolf et al., 2016), thereby providing a spatial framework under which, for example, links between physical and ecological processes can be investigated (Frissell et al., 1986; Naiman, 1998), hypotheses regarding the impacts of landscape disturbance can be developed and tested (Buffington and Montgomery, 2013), reaches suitable for rehabilitation can be identified (Brierley and Fryirs, 2000), and river restoration designs can be developed and implemented (Rosgen, 1994). This is achieved through the measurement of a variety of physical properties (increasingly quantified across different scales), selected on the basis that they are somehow reflective of the underlying processes that determine the appearance and behaviour of the river at a given point.

There has been considerable debate over the appropriateness of certain river classification schemes for applications in river management (Simon et al., 2007; Lave, 2009), with criticism centred on their lack of direct measurement of process rates, together with insufficient recognition of the importance of catchment and historical context (Montgomery and Buffington, 2013). Nevertheless, recent analysis by Kasprak et al. (2016) has shown that there can be widespread agreement between the outputs of different classification frameworks that have varying degrees of sophistication and data requirements when applied in the same catchment, suggesting some of these concerns may be overstated and that meaningful inference of fluvial processes can be

achieved through relatively straightforward quantification of form-based parameters. While this is encouraging, the vast majority of existing classification schemes are difficult to apply in situations where field measurement is dangerous and/or impractical, secondary data on channel morphology, grain size, etc. are either not available or spatially limited, and/or a large number of rivers need to be classified. They also fail to take full advantage of the improved variety and coverage of geomorphologically-relevant data that emerging technologies are generating. Google Earth provides an enormous, freely available data source that could be exploited for investigating many aspects of river environments; this research specifically explores whether it can support discrimination of river types through the extraction of form-based process indicators.

Research aims

In this paper, we explore the degree to which data sets describing process-relevant dimensional and morphological characteristics of rivers can be extracted from Google Earth via its Google Earth Pro software application. We test the utility of this information by investigating whether it can be used to develop a geomorphologically-meaningful, empirically-based classification of European semi-natural rivers, focussing mainly on single thread and transitional river planform styles. Our empirically-based analysis is bottom-up, allowing observed form-based process indicators to drive the classification rather than applying any *a priori* discrimination rules (for example, differentiating between river reaches on the basis of a predetermined sinuosity threshold). We then test the outcomes of the classification by examining the characteristics and distribution of the river classes identified through our analysis in relation to known independent controls of river form including reach-

scale energy and valley confinement conditions, thereby exploring the extent to which process can be inferred from form.

METHODS

Reach selection

In order to test the degree to which meaningful morphological features and dimensions can be extracted from Google Earth, sites displaying single thread or transitional planform styles (the planform types that dominate in Europe, Tockner et al., 2009) were selected for analysis which were also:

(i) as morphologically intact and free to adjust as possible. This was achieved by identifying river sites that appeared to be unconfined by buildings, infrastructure and channel training works such as embankments. Because of the widespread modification of European rivers, sites where up to 10 % of the channel length was affected by engineering structures were permitted, although virtually all selected sites showed a negligible extent of such interventions. However, it is important to note that not all modifications are apparent from a planview image and thus some selected sites may have greater modification than was anticipated;

(ii) located at sites with unregulated flow regimes. All sites displayed little evidence of large dams upstream, although one was located downstream of what appeared to be a large natural lake and another was close to an upstream weir. However, evidence of considerable flow and sediment dynamics in the sequence of available images suggested that this structure was probably quite low and/or imposed minimal flow and sediment regulation on downstream reaches. Most sites were located within 30 km of

a river flow gauging station that had been deemed to have a near-natural flow regime (Stahl et al., 2010). The list of gauging stations emanated from a European research programme (FRIEND) that did not include all countries within Europe. As a result, not all European countries were represented among the selected sites and only a few sites were included from countries that were not part of the FRIEND programme;

(iii) represented by at least one cloud free, high resolution image since 2000, which appeared to show the river under baseflow conditions to maximise the potential to identify in-channel features.

These reach selection criteria were designed to ensure that, as far as practically possible, morphological features and dimensions could a) be easily identified and b) would be reflective of a process regime not significantly affected by anthropogenic activity. 68 suitable sites were identified (Figure 1) on different European rivers and up to three reaches (each with a length exceeding 70 active widths) were selected for analysis within each site, giving a total of 194 reaches from which dimensional and morphological information could be extracted. A minimum reach length of 70 active widths was used to maximise opportunities for feature identification and reduce the effect of any vertical inaccuracy in elevation data on derived slope values. The mean reach length was 7.2 km.

Feature extraction and processing

A list of channel dimensions and associated indices (Table 1) and morphological features (Table 2) was assembled that had both process relevance and the potential to be extracted from Google Earth imagery and digital elevation data. Rules for feature

identification were developed iteratively by inspecting images of many river reaches until a stable set of features and identification rules was established. This set of features was then extracted for each of the 194 reaches.

Morphological feature frequency is affected by the dimensions of the river reach in which the features are located, including the reach length (the longer the length, the greater the expected number of any particular feature) and also river width (the wider the river, the smaller the expected number of any particular feature within a particular length of reach). Therefore, morphological feature frequency measurements were standardised to allow for the size of each sampled reach by multiplying each feature frequency by the ratio of active channel width to active reach length.

When extracting river dimensions and features at each site, the available images were inspected and the image that appeared to represent the lowest flow was typically used for the feature count. However, in some cases other criteria had to be considered. Cloud cover or heavy shading sometimes obscured significant lengths of river, in which case an alternative image or both images were used for feature extraction. In addition, a few reaches had been recently affected by engineering interventions and so earlier, pre-intervention images were used for feature extraction.

Classification of river reaches

Principal Components Analysis (PCA) was used to investigate the nature of any channel dimensional and morphological gradients present in the 194 reach data set. PCA was performed on a Spearman's ρ correlation matrix and a varimax rotation with Kaiser normalisation was applied to the set of PCs with eigenvalues greater than one,

to align them as closely as possible to the original variables and thus aid interpretation of the environmental gradients that the PCs described. Correlation coefficients for pairs of input variables and the results of Kaiser-Meyer-Olkin and Bartlett's sphericity tests were examined prior to PCA to ensure the selection of variables was robust and sampling was adequate.

Agglomerative hierarchical clustering (AHC) using Ward's algorithm was then applied to the reach scores on the varimax-rotated PCs. Reaches were assigned to different classes according to a natural break in the dendrogram based on the entropy level. The distinctiveness of the resultant reach class clusters was then validated statistically using Kruskal-Wallis (KW) tests followed by multiple pairwise comparisons, based on Dunn's procedure with Bonferroni correction. Qualitative descriptions of each class of river were then developed through examination of trends in bi-plots of reach PC scores and the results of the pairwise comparisons. All analyses were conducted using the 2018 version of XLSTAT Pro (http://www.addinsoft.com).

Geomorphological 'realism' of the classification

The degree to which the classification enabled discrimination of reaches subject to different process regimes was evaluated through examination of the distribution of reaches in each class in relation to variables describing known independent controls of river morphology and behaviour. Local energy conditions (as a proxy for sediment transport capacity and potential for morphological adjustment) were represented using a combination of valley slope (calculated using reach elevation data and valley length measurements from Google Earth) and a representative flood discharge. Valley slope was used instead of a measure of channel slope (e.g. Leopold and Wolman, 1957) as

it is independent of channel sinuosity and, thus, river class (Ferguson, 1984; 1987). For the majority of reaches (145), long flow gauging station records (>19 years in most cases) were available to estimate the two-year return period flood discharge (Q_2). This hydrological parameter was selected on the basis that it is also independent of channel morphology (van den Berg, 1995). Bankfull discharge has been commonly used as an explanatory variable in studies of river pattern (e.g. Leopold and Wolman, 1957) as it is considered to approximate the dominant (or effective) discharge that is theoretically representative of the full range of flows that determine sediment transport and morphological configuration in a given channel (Hey and Thorne, 1986). However, it is sensitive to changes in width:depth ratio (and, therefore, river class), is routinely estimated in a number of different ways and is not readily available at many locations (van den Berg, 1995). For a small number of reaches where flow data were not available, a literature-sourced estimate of the bankfull discharge was used as a substitute on the basis that it is comparable in magnitude to Q_2 for many rivers (Knighton, 1998).

Following Kleinhans and van den Berg (2011), these variables were combined to compute a potential specific stream power (W m^{-2}), ω_{pv}, designed to represent the energy available to perform geomorphic work in a given reach (Ferguson, 1987):

$$\omega_{pv} = \frac{\rho g Q S_v}{W_r} \quad (1)$$

where ρ = water density (kg m^{-3}), g = acceleration due to gravity (m s^{-2}), Q = reference discharge (m^3 s^{-1}) (two year return period flood or bankfull discharge), S_v = valley slope (m m^{-1}) and W_r = reference channel width (m). A reference, rather than actual, width

is used in the calculation so as to remain independent of channel type (see van den Berg, 1995, and Kleinhans and van den Berg, 2011, for detailed discussion of the merits of this approach). It is calculated using a regime equation:

$$W_r = \alpha\sqrt{Q} \quad (2)$$

with a coefficient of α = 3.0 $\sqrt{s\ m^{-1}}$ used in this application (Kleinhans and van den Berg, 2011).

The computation of ω_{pv} allowed the relationship between local energy conditions and descriptors of channel morphology (e.g. active channel width, sinuosity, etc.) derived from Google Earth to be explored. Previous research (Antropovskiy, 1972, cited in Alabyan and Chalov, 1998; van den Berg, 1995; Bledsoe and Watson, 2001; Kleinhans and van den Berg, 2011) has demonstrated that channel-independent measures of stream power can prove effective in discriminating between, and supporting interpretation of, different types of meandering and braided channels when bed material grain size is accounted for. The distribution of a subset of river reaches classified in this study (for which grain size data were available) was evaluated in relation to the following channel type discriminators from this published work:

$$\omega_{bm} = 900\ {D_{50}}^{0.42} \quad (3)$$

where D_{50} = median bed material grain size (m) and *bm* refers to a threshold between highly braided and meandering channels (van den Berg, 1995);

$$\omega_{sc} = 285\ {D_{50}}^{0.42} \quad (4)$$

where *sc* refers to a threshold between active meandering channels that exhibit scroll bars and those which exhibit chute (and scroll) bars (Kleinhans and van den Berg, 2011); and

$$\omega_{ia} = 90\ {D_{50}}^{0.42} \quad (5)$$

where *ia* refers to a threshold between laterally inactive channels and active meandering channels with scroll bars (Makaske et al., 2009).

Elevation and valley confinement conditions (as proxies for the potential significance of colluvial processes and restrictions on lateral mobility) were also quantified. Reach elevation was measured directly from Google Earth at the upstream boundary. Level of confinement was approximated by the proportion of the bank length that appeared to be in contact with valley side slopes and any high (ancient) terraces: reaches were deemed to be confined when more than 90% of the river bank length was in contact; unconfined when less than 10% of their river bank length was in contact; and partly confined where an intermediate level of bank contact was evident (Brierley and Fryirs, 2005).

RESULTS

Classification and characteristics of river reaches

Principal Components Analysis was performed on a Spearman's rank correlation matrix for 13 variables (Tables 1 and 2). Four variables represented river channel

dimensions: active channel sinuosity, the ratio of baseflow to active channel sinuosity, the ratio of median active to median baseflow channel width, the coefficient of variation of active channel width. These variables were selected to illustrate the planform character of the river reaches independently from their size. The remaining nine variables were counts of the physical features listed in Table 2 once they had been standardised for the length and width of the active channel.

The first four PCs all had eigenvalues greater than 1, indicating that they explained more of the variance in the data set than the original variables (Table 3). A varimax rotation of these four PCs simplified the structure of the loadings matrix and supported interpretation of the environmental gradients that they described. Focussing mainly on those variables with loadings $\geq$ 0.7 (Table 3), PC1 describes a gradient from reaches with little variation in width or sinuosity with increasing flow stage (positive loadings of 0.827 on Active:Baseflow channel width and 0.816 on Baseflow:Active channel sinuosity, respectively) and also limited longitudinal variability in their width (positive loading of 0.692 on Coefficient of variation of active channel width), to those with active channels that are distinctly wider and less sinuous than their baseflow channels, containing increasing numbers of active lateral and mid channel bars (positive loadings of 0.910 on Active lateral bar and 0.800 on Active mid-channel bar, respectively). The remaining three PCs describe gradients of increasing frequency of Active point bars and Channel cutoffs (PC2), increasing frequency of Bedrock and Rapids (PC3), and increasing frequency of Cascades and Steps (PC4). Finally, although the loading is relatively weak (-0.614), Riffles show a negative loading on PC4.

Agglomerative hierarchical clustering on the reach PC scores using Ward's algorithm and an entropy-based solution resulted in the identification of five clusters, each representing a different class of river reach (Figure 2). Classes A and B were found to be most similar in terms of their characteristics and, together with class C reaches, formed a higher level grouping that was dissimilar from classes D and E. Kruskal-Wallis tests followed by multiple pairwise comparisons, based on Dunn's procedure with Bonferroni correction, were used to establish which clusters showed significant differences in their scores on each of the PCs (Table 4). All five clusters were found to be fully discriminated by these analyses, with each cluster showing a significant difference from the others in relation to the scores on at least one PC. The distribution of the five classes with respect to the four PCs is illustrated in Figure 3. There is separation of classes B, C and E from class A along PC1 (Figure 3A) and class D from the other classes along PC 3 (Figure 3B). Furthermore, class B is discriminated from the other classes by PC2 (Figure 3C) and, apart from a group of outliers in class D, class E is distinguished from the other classes by PC4 (Figure 3D).

Based on the variables with high loadings on each PC (Table 3) and significant differences identified between the scores of reaches within the five classes on each PC (Table 4), Table 5 provides a summary interpretation of the five classes, along with an example reach from the centre of each cluster for visualisation purposes. In more detail, the classes are interpreted as follows:

Class A: Laterally stable channels with an absence of visible instream depositional features, and very limited variability in either width or sinuosity with increasing flow stage, or in width along their length.

Class B: Laterally active sinuous-meandering channels with visible point bars and cutoffs that become wider and less sinuous with increasing flow stage, and which vary in active width along their length.

Class C: Transitional (near-braided) channels with visible lateral and/or mid-channel bars with intervening riffles, which become wider and less sinuous with increasing flow stage, and which vary in width along their length.

Class D: Bedrock channels with visible rapids and, in some cases, cascade and/or step features. Low to intermediate variation in channel width or sinuosity with flow stage and the presence of occasional bars.

Class E: Cascade/step dominated channels with occasional lateral and/or mid-channel bars and an absence of visible point bars, riffles and exposed bedrock. Intermediate to strong variation in width both longitudinally and with increasing flow stage.

Relationships between channel morphology and independent control variables

The relative frequencies of fully, partly and unconfined reaches in each of the five river classes are shown in Figure 4. The majority of laterally stable and laterally active sinuous-meandering reaches (classes A and B) are unconfined (85% and 97%, respectively), with the remainder being partly confined. The valley confinement settings of transitional channel (class C) reaches are more varied, with 51% being unconfined, 38% partly confined and 10% fully confined. Bedrock channels (class D)

and, particularly, cascade/step dominated (class E) reaches are typically located in fully confined valley settings, accounting for 55% and 73%, respectively, of each class. Amongst bedrock channel (class D) reaches, 20% are in partly confined valley settings and 25% are unconfined. In comparison, only 7% of cascade/step dominated (class E) reaches are unconfined, with the remainder (20%) located in partly confined valley settings.

Cascade/step dominated (class E) reaches are situated at significantly higher elevations (all greater than 500 m and the majority above 1000 m) than reaches in the other four classes (Figure 5). Laterally stable (class A) and laterally active sinuous meandering (class B) reaches tend to be found at much lower elevations (median = 92 m and 133 m, respectively). The average height of transitional (class C) and bedrock (class D) channel reaches is similar (median = 277 m and 124 m, respectively) but reaches in these classes occupy a wider range of elevations from near sea-level up to approximately 1000 m and 2300 m, respectively.

The distribution of reaches in the five river classes with respect to Q_2 and valley slope is illustrated in Figure 6. There is notable overlap between some of the classes, particularly for transitional (class C) and bedrock (class D) channels, but others occupy relatively discrete areas of the plot. Cascade/step dominated (class E) reaches are grouped in the upper left region of the plot, with contrasting high valley slopes but relatively low discharges. Bedrock channel (class D) reaches tend to occupy the centre and right of the plot, with relatively high slopes or high discharges, in a similar zone to most of the transitional channel (class C) reaches. The bottom left region of the plot is exclusively occupied by laterally stable (class A) reaches, which persist with increasing

slope and/or discharge towards the centre. Laterally active sinuous-meandering (class B) reaches occupy a zone that combines intermediate slope and discharge.

Figure 7 illustrates the range of potential specific stream power values of reaches of different classes for which an estimate of bed material grain size was available and shows their distribution relative to empirically-derived thresholds between alluvial channels types derived using Equations 3-5. Laterally stable (class A) reaches occur at a wide range of potential specific stream powers, existing under conditions where no lateral movement or bar formation would be expected but also those potentially capable of instigating scroll and chute bar development and even active braiding. Transitional (class C) channels are almost exclusively restricted to a range of potential specific stream power values above the threshold required for meandering with scroll and chute bar development and moderate braiding but below that required for significant levels of braiding. Laterally active sinuous-meandering (class B) reaches span a domain above the potential specific stream power threshold required for scroll bar development but below that above which highly braided rivers occur.

Figures 8a and 8b highlight the existence of complex associations, at class level, between potential specific stream power and morphological parameters (channel width and sinuosity) typically used in other classifications but which did not explicitly inform the groupings identified above. The active widths of laterally stable (class A) channels tend to be narrower than those of laterally active sinuous meandering (class B) and transitional (class C) reaches for a given potential specific stream power. The active channels of cascade/step dominated (class E) reaches are relatively narrow in comparison to reaches from other classes apart from laterally stable (class A)

channels, albeit at much greater potential specific stream powers, while the active widths of bedrock (class D) channels are more variable. A general trend of declining active channel sinuosity with increasing potential specific stream power is evident from laterally active sinuous-meandering (class B), through transitional (class C) and bedrock (class D), to cascade/step dominated (class E) channel reaches. However, laterally stable (class A) channels exhibit a wide range of sinuosity values that appear to be unrelated to local energy conditions.

DISCUSSION

Extraction of geomorphologically-relevant information from Google Earth images

Our analysis of information extracted from Google Earth Pro has yielded a classification of river types that not only appears geomorphologically-intuitive but confirms previously hypothesised associations with independent data sets that describe a set of controlling variables. Nevertheless, there are a number of issues that constrain how far and at what resolutions geomorphologically-relevant data can be extracted from Google Earth.

The level of detail achieved by the geomorphological classification of European rivers presented herein is largely determined by the types of process indicators that can be resolved from Google Earth images and the accuracy with which they can be measured or counted. The potential significance of these factors is a function of the number, timing and resolution of the available images in the Google Earth database for a given reach. An expanded list of potential process indicators was originally considered for the study, including a more comprehensive suite of bar types,

vegetation types and associated morphological units including benches, and instream assemblages of large wood. This could, in theory, have led to the isolation of further groupings or sub-types of reaches but these features proved difficult to reliably identify as a result of the lack of control on flow stage and/or season at the time of image capture, water clarity issues and/or obscuration by riparian trees. Wherever possible, we worked on images that appeared to represent baseflow conditions, but of course we cannot be sure that we had acceptably comparable flow levels in all of the images we analysed. This was a particular issue where the number of clear images was small, since this prevented comparisons to confirm differences in stage. This issue underpinned our decision to rely more heavily on active channel dimensions in our analysis, since these were more consistently identified using the edge of continuous vegetation cover as the criterion. In addition, where only summer images could be analysed or where image resolution was low, riparian vegetation could have adversely affected all data extraction, but particularly the identification of smaller or more nuanced in-channel physical features.

The procedures for identifying and measuring or counting the process indicators utilised in this study were completed manually. The pan, zoom and path measurement tools available in Google Earth Pro make this a relatively straightforward task but it is time-consuming to complete for a large sample of river reaches and introduces the potential for human error. Recent developments in image processing technology and increasing provision of freely-available remotely sensed data products could facilitate the semi- or complete automation of the geomorphological classification approach proposed in this paper. The release of Google's Earth Engine cloud computing platform in 2010 has provided the research community with both access to remotely

sensed imagery and the computational power required to process such data at the global scale (Gorelick et al., 2017). It has enabled analyses with a spatial and temporal richness that would previously have been considered unachievable, including tracking surface water dynamics (Pekel et al., 2016), quantifying the status and distribution of sensitive habitats (Giri et al., 2010) and monitoring urban development (Patel et al., 2015). To date, this research has largely been centred on the use of data from NASA's Landsat and ESA's Copernicus programmes but neither platform offers the spatial resolution necessary to resolve the types of features used in this study. However, this situation is changing with the emergence of increasingly high resolution geospatial data products. The recent release of Planet's SkySat imagery via Google Earth Engine, offering true colour imagery at sub-metre resolution and multispectral imagery at 2 m resolution, could enable the accurate automated delineation of channel boundaries and geomorphic units. The process of identifying and extracting geomorphologically-relevant information from this high resolution imagery would not be an insignificant task but comprehensive taxonomic frameworks for the identification of a huge range of fluvial landforms already exist (e.g. Wheaton et al., 2015), image processing workflows capable of extracting channel networks and their geometric properties have been developed (e.g. Isikdogan et al., 2017; Monegaglia et al., 2018), and object-based image analysis techniques have great potential for identifying spatially-distinctive features (e.g. Demarchi et al., 2016; Demarchi et al., 2017). We encourage further research towards the goal of operationalising such methods for global application in the field of river classification.

Geomorphological 'realism' of the classification

We have explored the utility of Google Earth as a source of geomorphologically-relevant information by developing a classification of transitional to single thread near-natural European rivers. The apparent 'realism' of this classification is one test of the utility of the extracted data on which it is based, but the classification is also dependent upon a number of other factors.

In addition to being influenced by the nature of data available through Google Earth, the reach types identified in this study were also determined to a certain degree by the sampling strategy employed. Our focus was on river reaches whose morphology was considered to be "in tune" with a natural process regime (i.e. not visibly affected by dams or other engineering activities). This immediately precluded many lowland systems from our analysis given their long history of management in Europe and, as a result, prevented the inclusion of a number of possible additional process indicators such as stable (vegetated) islands as they would have been present in such low quantities across the sample of 194 reaches that their inclusion would have compromised the PCA undertaken. The same is true of natural large braided rivers, which were once common across the Alps and other mountainous regions of Europe but have been heavily impacted by flow regulation, gravel extraction and erosion control measures (Tockner et al., 2003). Together, this accounts for the absence of several "classic" river types (e.g. anastomosing, fully braided, etc.) that would potentially have emerged from the classification procedure had it been undertaken on rivers in other parts of the world.

It is also important to acknowledge that, despite our best efforts to only sample river reaches that did not have any obvious artificial constraints on their adjustment for

analysis, this is not straightforward when working with planview aerial imagery. In particular, bank reinforcement is rarely visible in these data products. Therefore, we cannot be sure that significant reinforcement was not in place, and on the larger, lowland rivers it is likely to have been present to some extent. In addition, in the few reaches where cross-channel structures were present, we ensured that they were limited in number but their vertical extent and thus potential impact on upstream and downstream dynamics could not be assessed. The presence of engineered structures in invidual reaches may have influenced the recorded process indicator values through their impacts on hydraulic and sediment transport processes and, thus, may have affected the allocation of reaches to particular classes.

Despite these caveats, the classification procedure resulted in the definition of five river reach types with distinctive geomorphological identities whose internal characteristics and distribution can be explained in relation to known independent controls on river form. Under low energy conditions in unconfined valley settings, laterally stable channels lacking visible instream depositional features and longitudinal variation in width, and which do not experience signficant changes in width or sinuosity with increasing flow stage, were found to dominate. These reaches tended to be relatively narrow in comparison to the other reach types found in unconfined settings. Such characteristics are consistent with those of suspended load-dominated channels with relatively low width-depth ratios and banks formed of highly resistant cohesive sediments. Under increasingly energetic conditions (but remaining in unconfined settings), reaches with those characteristics were still observed but became less common relative, firstly, to laterally active sinuous-meandering channels and then, at even greater values of ω_{vp}, transitional (near-braided) channels. The fact that laterally

stable channels are able to persist under high energy conditions is perhaps initially surprising but it is important to remember that it is the strength of the erosive force relative to the resistive strength of the boundary that ultimately determines channel mobility (Huang et al., 2004). Closer visual inspection of a sample of laterally stable reaches at the upper end of the energy gradient revealed the presence of mature riparian trees along their banks. Riparian vegetation can be highly effective in increasing the stability of river banks through both its effect on near-bank hydraulic roughness (Tooth and McCarthy, 2004) and by binding sediments together (Holloway et al., 2017). These processes or, potentially, the presence of undetected bank erosion control structures may explain the occurrence of this type of reach under high energy conditions.

The occurrence of laterally active sinuous-meandering reaches with visible point bars and cutoff features that vary longitudinally in width and become wider and less sinuous with increasing flow stage was found to be consistent with situations where local hydraulic conditions are sufficiently energetic to mobilise bedload material and overcome the resistive strength of the channel boundary. When bed material grain size was taken into account, these reaches were found to occur at ω_{vp} values between empirically defined thresholds for the onset of meandering with scroll bar development (Makaske et al., 2009; Equation 5, Figure 5) and below those required to instigate high levels of braiding (van den Berg, 1995; Equation 3, Figure 5). They were found in unconfined settings and were generally significantly wider than laterally stable reaches. It is important to note that these reaches could not have been isolated on the basis of their sinuosity alone (c.f. early classification schemes such as that of Leopold and Wolman, 1957). A large number of laterally stable reaches had similar, and

occasionally greater, sinuosity values than those of the laterally active sinuous-meandering reaches identified in this study. However, as discussed above, river energy is not the only determinant of meandering and this is evident from the lack of any clear, systematic correlation between ω_{vp} and sinuosity. Inactive meandering channels have been shown to exist as a product of antecedent relief (e.g. Kleinhans et al., 2009) or as relic features formed under different process regimes (e.g. Ferguson, 1987). This highlights the danger of classifying reaches based on simple, individual measures of channel form. Without the inclusion of visual observations of point bar features, longitudinal width measurements and consideration of channel form under baseflow and active conditions as part of the classification procedure, process-based distinction between different types of "meandering" rivers would not have been possible.

Transitional (near-braided) channels exhibiting lateral and/or mid-channel bars that become signficantly wider and less sinous with increasing flow stage were found to occur almost exclusively under high energy conditions and above an empirically-derived threshold for the onset of meandering with scroll and chute bar development and moderate braiding (Kleinhans and van den Berg, 2011; Equation 4, Figure 5). The average active width of reaches in this class was found to be significantly greater than that of laterally stable reaches. This is consistent with channel development in situations were local hydraulic forces significantly exceed the resistive strength of the channel boundary. The strong contrast between the morphological configuration of these two reach classes is shown in Figure 9. It compares the measured width of reaches in each class with their expected width based on Equation 2. The equation (originally derived from a data set of largely single-thread gravel bed rivers)

systematically predicts much greater width values for laterally stable reaches than were measured, pointing to the likely highly resistive nature of their bank materials. However, transitional channels are predicted to be narrower than measured, indicating a highly erodible boundary. Closer inspection of a sample of our study reaches confirmed the presence of non-cohesive bed and bank materials. While the majority of the transitional reaches identified through the classification procedure were found in unconfined situations, they also occurred in confined and partially confined valleys. This is not unusual, with many gravel bed rivers in mountain environments adopting a "string-of-pearls" morphology, with intensely braided sections where valleys have infilled with coarse sediment and intervening single-thread or wandering sections where bedrock constraints restrict the valley width (Gurnell et al., 2000). This may partially account for the high longitudinal width variation evident in this reach class.

The remaining two reach types identified by the classification, bedrock and cascade/step dominated channels, were both predominantly found in confined valley situations and under very high energy conditions (primarily driven by steep valley slopes). This natural lateral constraint acts as a major control on channel width and sinuosity in both of these types of channels (Brierley and Fryirs, 2005) but their distinction here is enabled by contrasting scores for particular process indicators which are reflective of differences in sediment supply conditions. The presence of cascades and step features, coupled with occasional lateral and/or middle channel bars and strong longitudinal variation in width is consistent with situations in which channel morphology is strongly influenced by sediment supply via hillslope processes and relatively infrequent but high magntiude flood events (Montgomery and Buffington, 1997). Cascade/step dominated reaches tended to occur at sigificantly higher

elevations than bedrock reaches, where the exposure of visible bedrock and the presence of rapid features is indicative of very high transport capacity relative to the level of sediment supply (Montgomery et al., 1996). Resistant bedrock and consequently low bedload transport rates would account for the low to intermediate variation in width or sinuosity with flow stage and only occasional presence of bar features.

Further applications of the use of form-based process indicators from Google Earth in river classification

The interpretability of the reach types derived in this study in relation to known controls of river morphology and behaviour suggests that form-based process indicators derived from Google Earth can provide a sound basis for river classification. While we acknowledge the importance of sources of error and limitations with the method presented, the results suggest that there are sufficiently strong links between river form and process to enable remote definition of geomorphologically-meaningful reach categories. The bottom-up nature of the method means reach types are not fixed but, instead, are determined by the data themselves. Repeating the classification on a completely different sample of rivers would not necessarily result in definition of the same five reach types and, in doing so, the approach respects the fact that river channels span a continuum without definitive, fixed thresholds between types (Ferguson, 1987; Church, 2006). It is also important to note that the resulting classfication does not have to represent an “end-point”. If available, supplementary information that is not attainable from Google Earth (e.g. field measurements of grain size, depth, etc.) could be used to further categorise reaches.

A key aim of this paper was to attempt to link channel reach types to potential underlying physical controls that were relatively simple to define using a combination of published data and Google Earth. However, there is a need to further validate the findings using field surveys of boundary materials in different reach types. Likewise, although beyond the scope of our study, the existence of an ever-expanding database of historical imagery in Google Earth offers great potential for developing dynamic form-based process indicators and tracking the temporal trajectories of individual reaches as a way of characterising their geomorphological sensitivity (Fryirs, 2017). Finally, the approach could be used to help prioritise reaches for conservation and restoration efforts by characterising the nature and distribution in relation to physical controls of heavily managed river reaches. They could be expected to display different process-indicator values when compared to near-natural reaches in similar physiographic settings. It raises the prospect that, as higher resolution data sets become available and semi-automation is enabled via platforms such as Google Earth Engine, reaches in disequilibrium could be quickly identified throughout catchments and at national scales.

CONCLUSION

In this paper, we have explored whether process-relevant dimensional and morphological characteristics of rivers can be extracted from Google Earth via its Google Earth Pro software application by developing a classification of transitional to single thread river types. A geomorphologically-meaningful, empirically-based classification of European semi-natural rivers was achieved, but it is important to stress that its results were dependent on several factors that influenced site selection, image selection and data extraction:

(i) *Careful selection of river reaches that were as free as possible of direct geomorphological or hydrological interventions*. For testing the classification using independent process data, we confined our search to reaches where a nearby flow gauging station had been deemed to monitor near-natural flows or where the reach could be seen to be unaffected by major river regulation structures;

(ii) *Careful selection of images to maximise the consistency, quality and accuracy of any measurements*. In particular, we selected images that represented baseflow conditions, displayed good water clarity and, where there was overhanging riparian vegetation, were captured on a date where leaf cover would not obscure the features that are to be identified or measured;

(iii) *Selection of process- and form-relevant properties that could be extracted reliably from images*. This involved iterative development of measurement approaches and the eventual rejection of several properties that proved too difficult to identify or to measure consistently.

Within the constraints of focussing on the single thread to transitional planforms that are characteristic of most of European river systems, five broad river types were identified which showed expected relationships with controlling variables. This demonstrates that if used carefully, the Google Earth information system provides a source of identifiable and measurable process-relevant dimensional and morphological characteristics of rivers, at least across the range of river sizes investigated (6 m to 210 m channel width). This suggests that this freely-available

information source has enormous potential for supporting geomorphological investigations across large and inaccessible areas and, by analysing multi-temporal images of the same sites, investigating river changes over time.

As we have shown, there are limits to the types of information that can be extracted such that field investigations cannot always be avoided. However, there is enormous potential to undertake valuable preliminary and complementary analyses to those conducted in the field. Understanding river form, function and dynamics and developing and monitoring management interventions all require investigations across a range of space and time scales. Google Earth provides an enormous free data source that can be mined easily from the geomorphologist's desk top across many such scales, supporting the assembly of large, reliable data sets in a very cost-effective way.

REFERENCES

Alabyan, A.M., Chalov, R.S. (1998) Types of river channel patterns and their natural controls. *Earth Surface Processes and Landforms*, 23, 467-474.

Alber A, Piégay H. 2011. Spatial disaggregation and aggregation procedures for characterizing fluvial features at the network-scale: Application to the Rhône basin (France). *Geomorphology* 125: 343-360.

Beechie, T.J, Liermann, M., Pollock, M.M., Baker, S., Davies, J. (2006) Channel pattern and river-floodplain dynamics in forested mountain river systems. *Geomorphology*, 78, 124-141.

Bizzi, S., Demarchi, L., Grabowski, R.C., Weissteiner, C.J., van de Bund, W. 2015. The use of remote sensing to characterise hydromorphological properties of European rivers. *Aquatic Sciences*, First online, DOI: 10.1007/s00027-015-0430-7

Beldsoe, B.P., Watson, C.C. (2001) Logistic analysis of channel pattern thresholds: meandering, braiding, and incising. *Geomorphology*, 38, 281-300.

Brierley, G.J., Fryirs, K.A. (2000) River Styles, a geomorphic approach to catchment characterization: Implications for river rehabilitation in the Bega catchment, New South Wales, Australia. *Environmental Management*, 25, 661-679.

Brierley, G.J., Fryirs, K.A. (2005) *Geomorphology and River Management: Applications of the River Styles Framework*. Oxford: Blackwell Publishing, 398pp.

Buffington, J.M., Montgomery, D.R. (2013) Geomorphic classification of rivers. In Shroder, J., Wohl, E. (eds.), *Treatise on Geomorphology*. San Diego: Academic Press, vol. 9, Fluvial Geomorphology, pp. 730–767.

Church, M. (2006) Bed material transport and the morphology of alluvial river channels. *Annual Review of Earth and Planetary Sciences*, 34, 325-354.

Demarchi, L., Bizzi, S., Piegay, H. (2016) Hierarchical object-based mapping of riverscape units and in-stream mesohabitats using LiDAR and VHR imagery. *Remote Sensing*, 8, 97.

Demarchi, L., Bizzi, S., Piegay, H. (2017) Regional hydromorphological characterization with continuous and automated remote sensing analysis based on VHR imagery and low-resolution LiDAR data. *Earth Surface Processes and Landforms*, 42, 531-551.

Farr, T.G., Rosen, P.A., Caro, E., Crippen, R., Duren, R., Hensley, S., Kobrick, M., Paller, M., Rodriguez, E., Roth, L., Seal, D., Shaffer, S., Shimada, J., Umland, J., Werner, M., Oskin, M., Burbank, D., Alsdorf, D. (2007) The Shuttle Radar Topography Mission. *Reviews of Geophysics*, 45, RG2004.

Ferguson, R.I. (1984) The threshold between meandering and braiding. *Channels and Channel Control Structures*, 6, 15–29.

Ferguson, R.I. (1987) Hydraulic and sedimentary controls of channel patterns. in K.S. Richards (ed.), *River Channels: Environment and Processes*. Oxford: Blackwell, pp. 129–158.

Frissell, C.A., Liss, W.J., Warren, C.E., Hurley, M.D. (1986) A hierarchical framework for stream habitat classification: Viewing streams in a watershed context. *Environmental Management*, 10, 199-214.

Fryirs, K. (2017) River sensitivity: a lost foundation concept in fluvial geomorphology. *Earth Surface Processes and Landforms*, 42, 55-70.

Giri, C., Ochieng, E., Tieszen, L.L., Zhu, Z., Singh, A., Loveland, T., Masek, J., Duke, N. (2010) Status and distribution of mangrove forests of the world using earth observation satellite data. *Global Ecology and Biogeography*, 20, 154-159.

Gorelick, N., Hancher, M., Dixon, M., Ilyushchenko, S., Thau, D., Moore, R. (2017) Google Earth Engine: Planetary-scale geospatial analysis for everyone. *Remote Sensing of Environment*, 202, 18-27.

Gurnell, A.M., Petts, G.E., Harris, N., Ward, J.V., Tockner, K., Edwards, P.J., Kollmann, J. (2000) Large wood retention in river channels: the case of the Fiume Tagliamento, Italy. *Earth Surface Processes and Landforms*, 2000, 25, 255-275.

Gurnell, A.M. Rinaldi, M., Belletti, B., Bizzi, S., Blameur, B., Braca, G., Buijse, T., Bussenttini, M., Camenen, B., Comiti, F., Demarchi, L., Garcia de Jalon, D., Gonzalez, del Tanago, M, Grabowski, R., Gunn, I., Habersack, H., Hendriks, D., Henshaw, A.J., Klosch, M., Lastoria, B., Latapie, A., Marcinkowski, P., Martinez-Fernandez, V., Mosselmann, E., Mountford, J.O., Nardi, L., Okruszko, T., O'Hare, M.T., Palma, M., Percopo, C., Surian, N., van de Bund, W., Weissteiner, C., Ziliani, L. (2016) A multi-scale hierarchical framework for developing understanding of river behaviour to support river management. *Aquatic Sciences*, 78, 1-16.

Hey, R.D., Thorne, C.R. (1986) Stable channels with mobile gravel beds. *Journal of Hydraulic Engineering*, 112, 671-689.

Holloway, J.V., Rillig, M.C., Gurnell, A.M. (2017) Underground riparian wood: Buried stem and coarse root structures of Black Poplar (Populus nigra L.). *Geomorphology,* 279, 188-198.

Huang, H.Q., Chang, H.H., Nanson, G.C. (2004) Minimum energy as the general form of critical flow and maximum flow efficiency and for explaining variation in channel pattern. *Water Resources Research*, 40, W04502.

Isikdogan, F., Bovik, A., Passalacqua, P. (2017) RivaMap: An automated river analysis and mapping engine. *Remote Sensing of Environment*, 202, 88-97.

Janes, V.J.J., Nicholas, A.P., Collins, A.L., Quine, T.A. (2017) Analysis of fundamental physical factors influencing channel bank erosion: results for contrasting catchments in England and Wales. *Environmental Earth Sciences*, 76, 307.

Kasprak, A., Hough-Snee, N., Beechie, T., Bouwes, N., Brierley, G., Camp, R., Fryirs, K., Imaki, H., Jensen, M., O'Brien, G., Rosgen, D., Wheaton, J. (2016) The blurred line between form and process: a comparison of stream channel classification frameworks. *PLoS ONE*, 11, e0150293.

Kleinhans, M.G., Schuurman, F., Bakx, W, Markies, H. (2009) Meandering channel dynamics in highly cohesive sediment on an intertidal mud flat in the Westerschelde estuary, the Netherlands. *Geomorphology*, 105, 261-279.

Kleinhans, M.G., van den Berg, J.H. (2011) River channel and bar patterns explained and predicted by an empirical and a physics-based method. *Earth Surface Processes and Landforms*, 36, 721-738.

Knighton, A.D. (1998) *Fluvial forms and processes. A New Perspective*. London: Edward Arnold.

Kondolf, G.M., Piegay, H., Schmitt, L., Montgomery, D.R. (2016) Geomorphic classification of rivers and streams. In G.M. Kondolf, H. Piegay (eds), *Tools in Fluvial Geomorphology*. Chichester: John Wiley & Sons Ltd, pp. 133-158.

Large, A.R.G., Gilvear, D.J. (2015) Using Google Earth, a virtual-globe imaging platform, for ecosystem services-based river assessment. *River Research and Applications*, 31, 406-421.

Lave, R. (2009) The controversy over Natural Channel Design: substantive explanations and potential avenues for resolution. *Journal of the American Water Resources Association*, 45, 1519-1532.

Leopold, L.B, Wolman, G.M. (1957) *River Channel Patterns: Braided, Meandering and Straight*. U.S Geological Survey Professional Paper 282-B, pp. 39–85.

Makaske B., Smith, D., Berendsen, H., de Boer, A., van Nielen-Kiezebrink, M., Locking, T. (2009) Hydraulic and sedimentary processes causing anastomosing morphology of the upper Columbia River, British Columbia, Canada. *Geomorphology*, 111, 194-205.

Marcus, A., Fonstad, M. 2010. Remote sensing of rivers: the emergence of a subdiscipline in the river sciences. *Earth Surface Processes and Landforms 35*:1867–1872.

Monegaglia, F., Zolezzi, G., Güneralp, I., Henshaw, A.J., Tubino, M. (2018) Automated extraction of meandering river morphodynamics from multitemporal remotely sensed data. *Environmental Modelling and Software*, 105, 171-186.

Montgomery, D.R., Buffington, J.M. (1997) Channel-reach morphology in mountain drainage basins. *GSA Bulletin*, 109, 596-611.

Montgomery, D.R., Abbe, T.B., Buffington, J.M., Peterson, N.P., Schmidt, K.M., Stock, J.D. (1996) Distribution of bedrock and alluvial channels in forested mountain drainage basins. *Nature*, 381, 587-589.

Naiman, R.J. (1998) Biotic stream classification. In R.J. Naiman, R.E. Bilby (eds), *River ecology and management: lessons from the Pacific Coastal ecoregion*. New York: Springer-Verlag.

Patel, N.N., Angiuli, E., Gamba, P., Gaughan, A., Lisini, G., Stevens, F.R., Tatem, A.J., Trianni, G. (2015) Multitemporal settlement and population mapping from Landsat using Google Earth Engine. *International Journal of Applied Earth Observation and Geoinformation*, 35, 199-208.

Pekel, J-F., Cottam, A., Gorelick, N., Belward, A.S. (2016) High-resolution mapping of global surface water and its long-term changes. *Nature*, 540, 418-422.

Rosgen, D.L. (1994) A classification of natural rivers. *Catena*, 22, 169-199.

Schmitt R, Bizzi S, Castelletti A. 2014. Characterizing fluvial systems at basin scale by fuzzy signatures of hydromorphological drivers in data scarce environments. *Geomorphology*. doi: 10.1016/j.geomorph.2014.02.024

Schumm, S.A. (1977) *The Fluvial System*. New York: Wiley, pp. 338.

Simon, A., Doyle, M., Kondolf, M., Shields Jr, F.D., Rhoads, B., McPhillips, M. (2007) Critical evaluation of how the Rosgen Classification and associated "Natural Channel Design" methods fail to integrate and quantify fluvial processes and channel response. *Journal of the American Water Resources Association*, 43, 1117-1131.

Stahl, K., Hisdal, J., Hannaford, J., Tallaksen, L., Van Lanen, H., Sauquet, E., Demuth, S., Fendekova, M., Jordar, J. (2010) Streamflow trends in Europe: evidence from a dataset of near-natural catchments. *Hydrology and Earth System Sciences*, 14, 2367-2382.

Tadaki, M., Brierley, G., Cullum, C. (2014) River classification: theory, practice, politics. *WIREs Water*, 1, 349-367.

Tockner, K., Ward, J.V., Arscott, D.B., Edwards, P.J., Kollmann, J., Gurnell, A.M., Petts, G.E., Maiolini, B. (2003) The Tagliamento River: a model ecosystem of European importance. *Aquatic Sciences*, 65, 239-253.

Tockner, K., Uehlinger, U., Robinson, C.T. (2009) *Rivers of Europe*. London: Elsevier, pp. 728.

Tooth, S., McCarthy, T.S. (2004) Anabranching in mixed bedrock-alluvial rivers: the example of the Orange River above Augrabies Falls, Northern Cape Province, South Africa. *Geomorphology*, 57, 235-262.

van den Berg, J.H. (1995) Prediction of alluvial channel pattern of perennial rivers. *Geomorphology*, 12, 259-279.

Wheaton, JM, Fryirs, KA, Brierley, G, Bangen, SG, Bouwes, N, O'Brien, G. (2015) Geomorphic mapping and taxonomy of fluvial landforms. *Geomorphology*, 248, 273-295.

ACKNOWLEDGEMENTS

The research for this paper was conducted within the SMART Joint Doctoral programme (Science for the MAnagement of Rivers and their Tidal systems) funded with the support of the Erasmus Mundus programme of the European Union. The authors would like to thank the National River Flow Archive (United Kingdom), Ministere de L'ecologie, du developpement durable et de l'energie (France), and Centro de Estudios Hidrograficos de CEDEX (Spain) for the provision of river flow records. Lastly and most importantly, the authors thank Google Earth and the many contributing companies who have provided the aerial imagery across Europe that has made this research possible, including Image Landsat, Infoterra Ltd and Bluesky, Getmapping plc, Digital Globe, IGN France, GeoBasis-DE/BKG, Cnes/Spot Image, Geoimage Austria, Eurosense/Geodis Slovakia, CNES/Austrium, MGGP Aero, Lantmaateriet/Metria, and Geodis Brno. Alan Kasprak and an anonymous reviewer provided valuable comments which helped strengthen this paper.

Figures

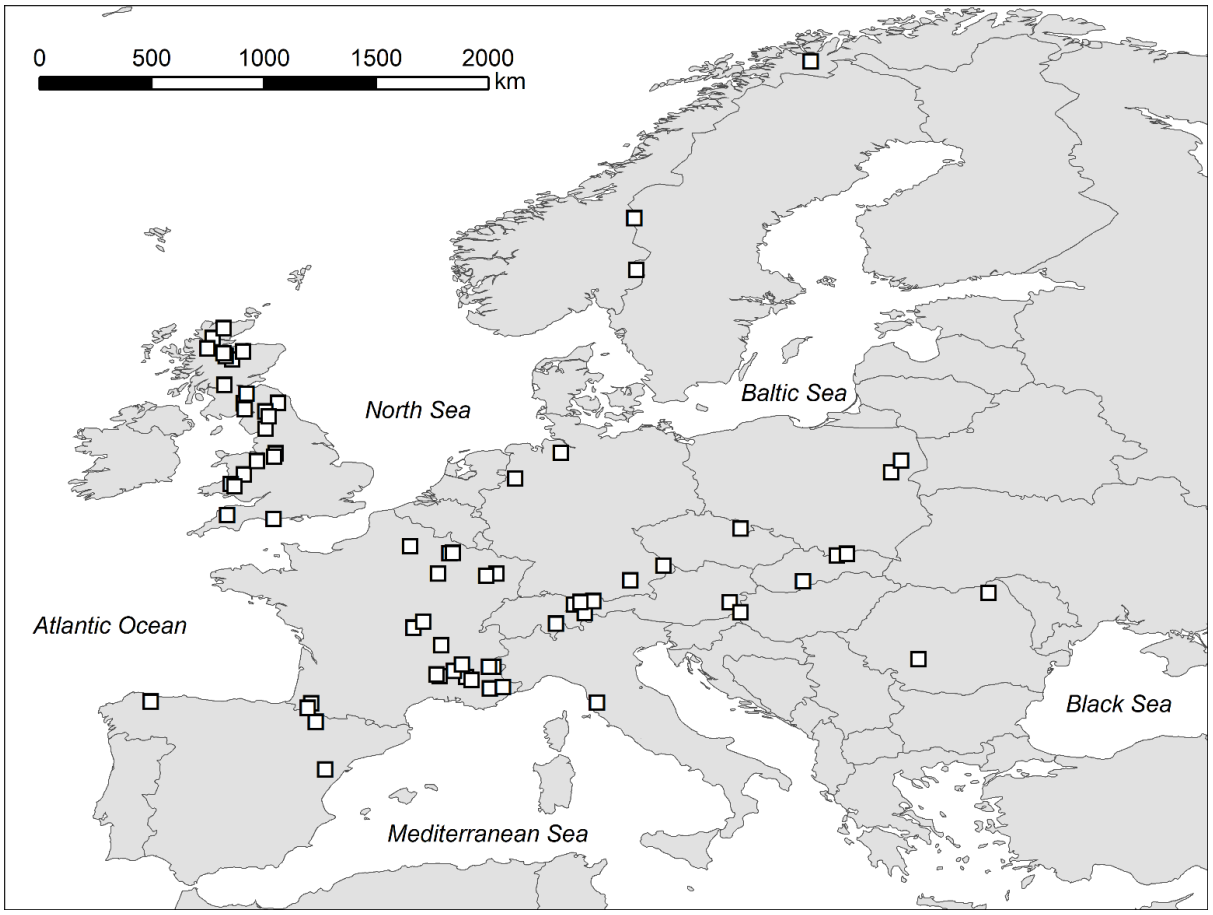

Figure 1: Locations of the 68 rivers from which data for 194 reaches were extracted.

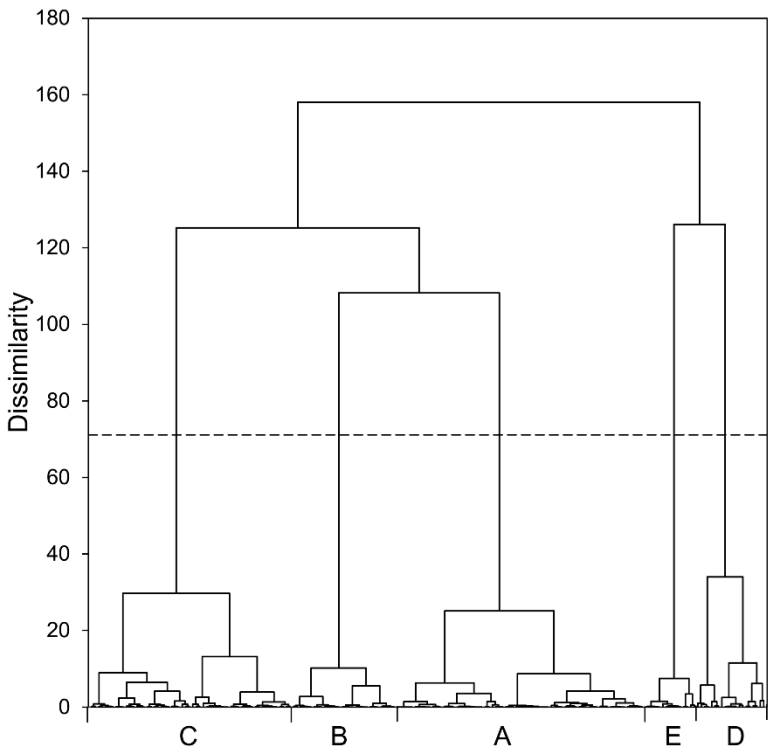

Figure 2: Dendrogram showing truncation (dashed line) of study reaches into five classes by AHC using Ward's algorithm and an entropy-based solution.

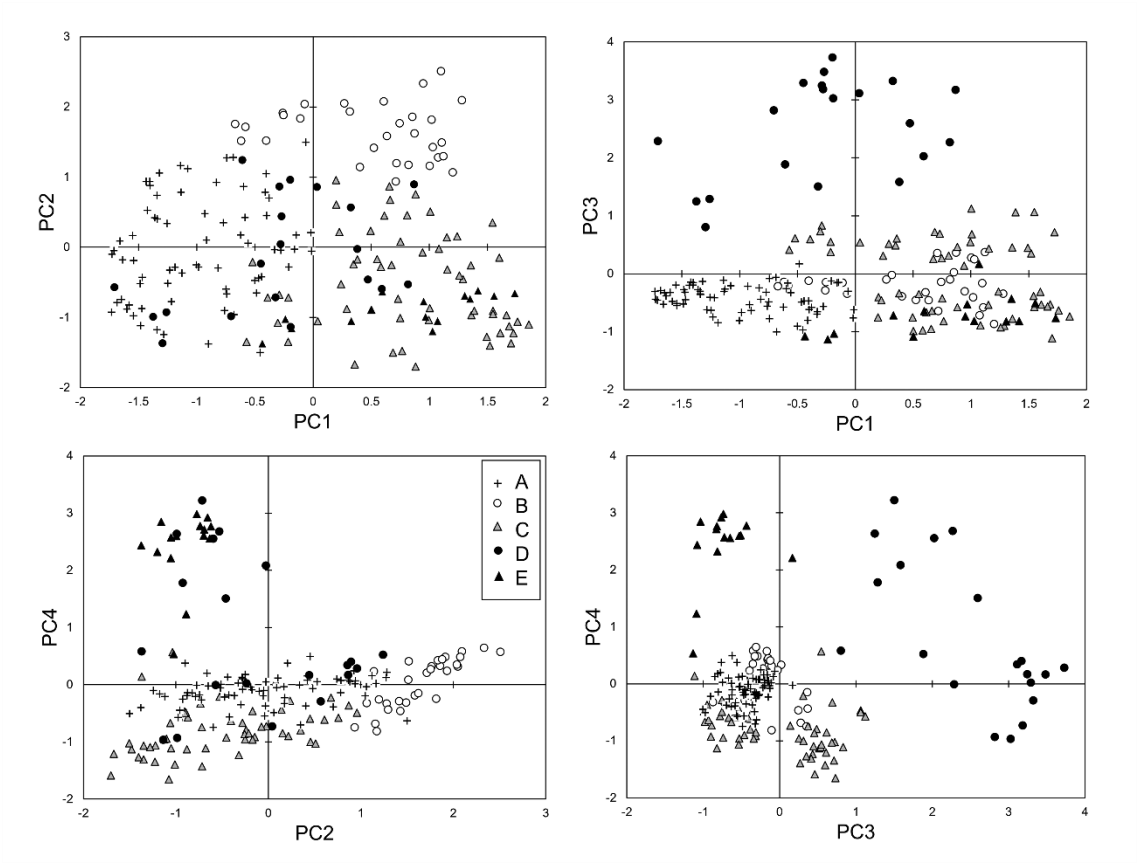

Figure 3: Scatter plots showing the distribution of the 194 reaches and their class membership with respect to PCs 1 to 4.

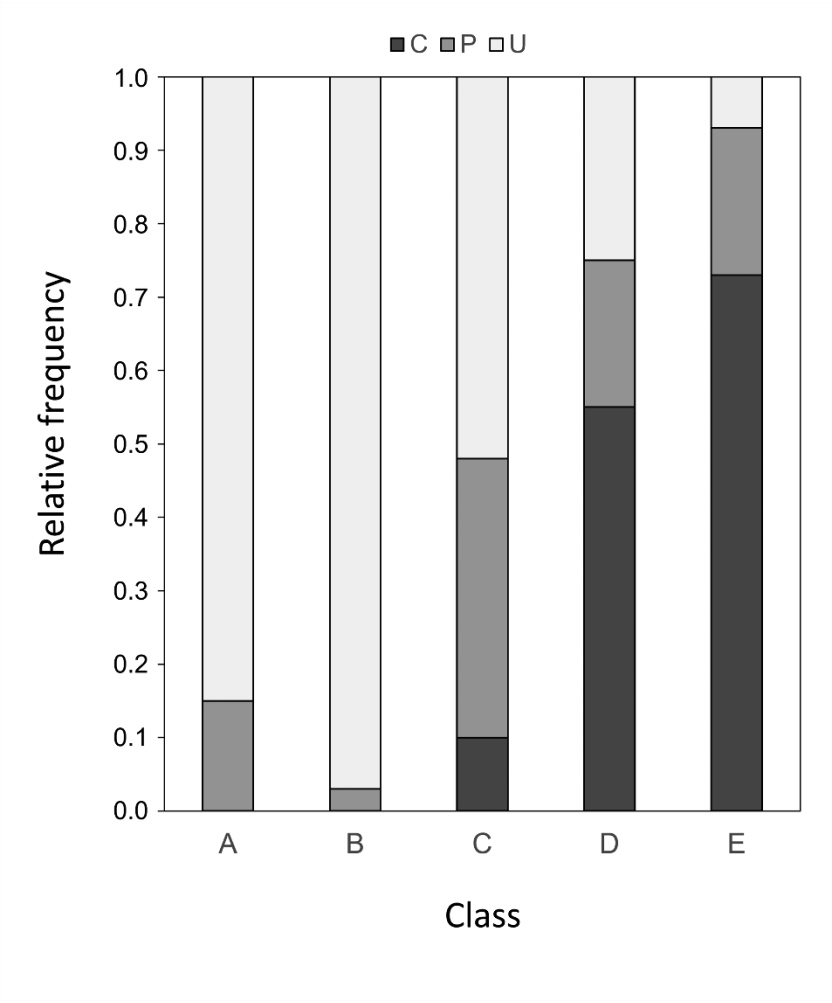

Figure 4: Frequency of fully (C), partly (P) and unconfined (U) reaches in each river class.

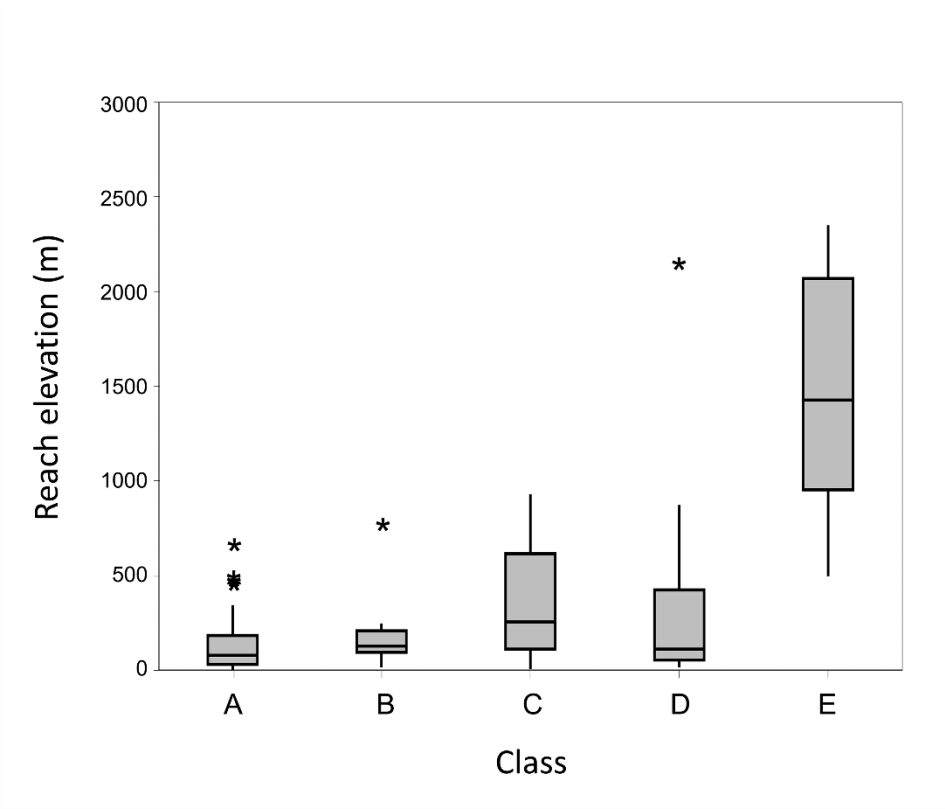

Figure 5: Distribution of reaches in each river class in relation to elevation.

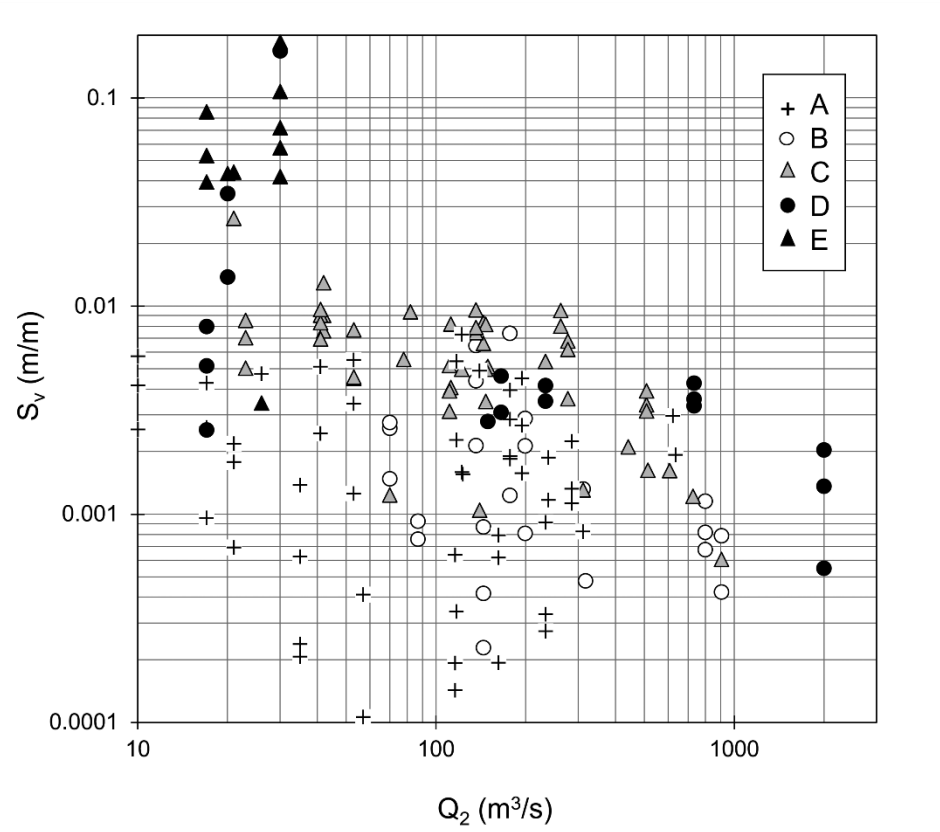

Figure 6: Distribution of reaches in each river class in relation to the two year return period flood discharge, Q_2, and valley slope, S_v.

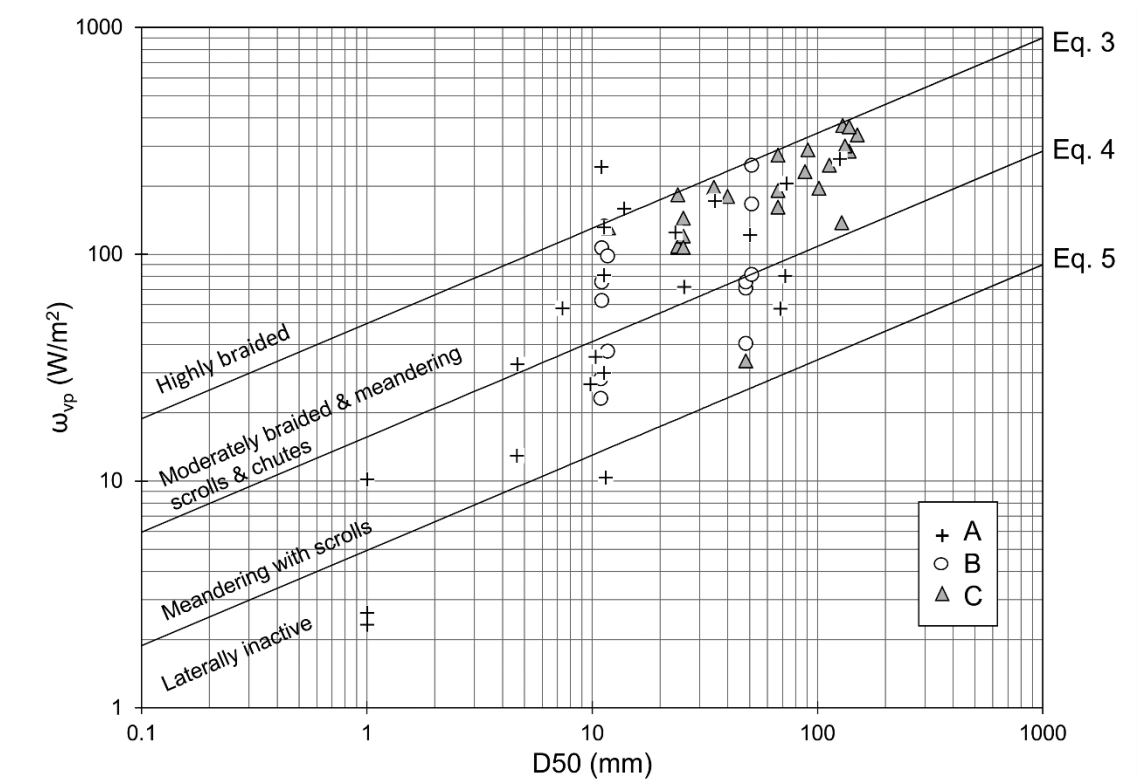

Figure 7: Distribution of reaches of different classes in relation to bed material grain size and potential specific stream power. Lines represent empirically-derived discriminators of channels types from van den Berg (1995), Kleinhans and van den Berg (2011) and Maskaske et al. (2009), respectively. Bed material grain size estimates were not available for any rivers in classes D and E.

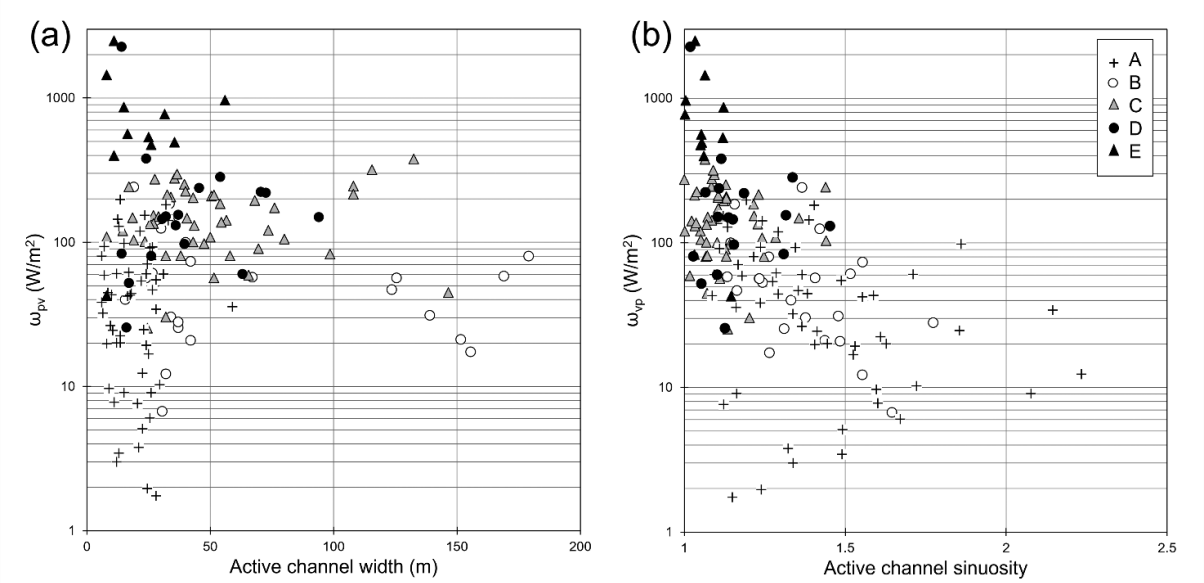

Figure 8: Relationships between potential specific stream power and a) active channel width; and b) active channel sinuosity.

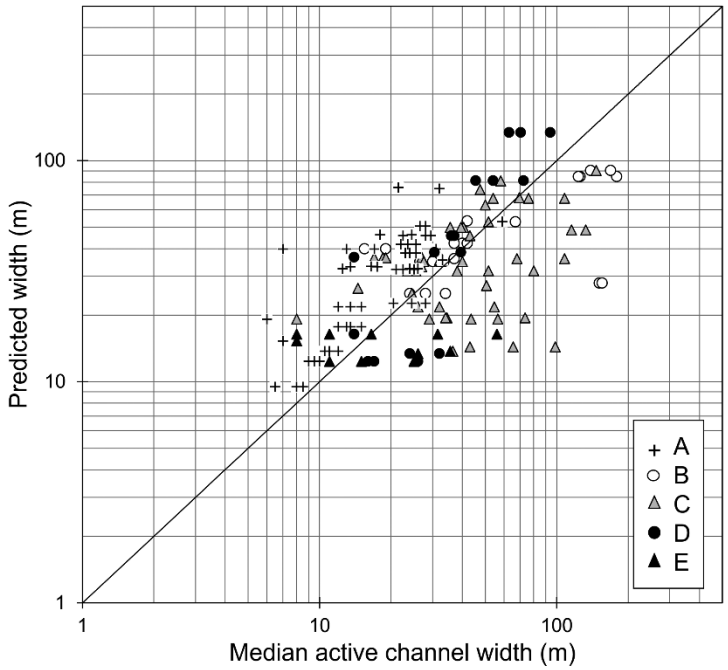

Figure 9: Comparison between measured active width and predicted width according to Equation 2 (from Kleinhans and van den Berg, 2011).

Tables

Dimension (units)	Description	Relationship to fluvial processes
Extracted from Google Earth		
Upstream elevation (m)	Elevation of the lower bank top at the upstream end of the reach.	
Downstream elevation (m)	Elevation of the lower bank top at the downstream end of the reach.	
Valley length (m)	Sum of straight line lengths between channel bend inflection points.	
Active reach length (m)	Mid-line length of channel whose edges are defined by continuous vegetation cover (unvegetated bars are part of channel width).	
Baseflow reach length (m)	Mid-line length of inundated channel at baseflow.	
Active channel width (m)	Width of the channel within the reach whose edges are defined by continuous vegetation cover (10 measurements taken at equally spaced intervals along the active channel mid-line).	
Baseflow channel width (m)	Water width (excluding exposed bars) at baseflow (2 measurements taken at locations where water width is at a minimum and maximum within the reach).	
Derived variables		
Active channel sinuosity	Active reach length / Valley length	
Baseflow channel sinuosity	Baseflow reach length / Valley length	
Active slope (m/m)	(Upstream elevation – Downstream elevation) / Active reach length	
Baseflow slope (m/m)	(Upstream elevation – Downstream elevation) / Baseflow reach length	
Valley slope (m/m)	(Upstream elevation – Downstream elevation) / Valley length	
Derived variables used in Principal Components Analysis		
Active channel sinuosity	See above	Capacity for lateral adjustment in meandering rivers (Janes et al., 2017)
Baseflow: Active channel sinuosity	(Baseflow reach length / Valley length) / (Active reach length / Valley length)	Indicative of bank erodibility relative to stream power and/or bed material supply rate (Carson, 1984; Ferguson, 1987).
Active: Baseflow channel width	(Median active channel width) / (Median baseflow channel width)	Proxy for width:depth ratio, indicates bank resistance relative to stream power (Eaton

		and Millar, 2004); response to changes in sediment load (Schumm, 1977); active (transporting) width (Garcia Lugo et al., 2015)
Coefficient of variation of active channel width	(Standard deviation of active channel width) / (Mean active channel width)	Strong longitudinal variation in channel width associated with increased morphological activity in meandering rivers that reflects variability in flow and sediment transport and bank material properties (Lagasse et al. 2004; Zolezzi et al., 2012)

Table 1: Channel dimensions extracted from Google Earth images and dimension indices used in Principal Components Analysis.

Feature	Description	Relationship to fluvial processes
Active lateral bar	Depositional feature attached to the river bank but not on the inside of a river bend with no significant vegetation cover and extending into the channel for at least 20% of the bankfull width.	Correlation between increasing frequency of bars and sediment supply rate (Brierley and Fryirs, 2005)
Active point bar	Depositional feature attached to the river bank on the inside of a river bend with no significant vegetation cover and extending into the channel for at least 20% of the bankfull width	Correlation between increasing frequency of bars and sediment supply rate (Brierley and Fryirs, 2005)
Active mid-channel bar	Mid-channel depositional feature with no significant vegetation cover that is not attached to the banks at normal flow and occupies a minimum of 20 % channel width	Presence indicates high rates of sediment supply and morphological activity (Brierley and Fryirs, 2005)
Channel cutoff	Recent or historic channel cutoff (can be wet or dry but is clearly visible on floodplain)	Presence indicates high rates of recent or historical morphological activity (Kleinhans and van den Berg, 2011)
Bedrock	Area of exposed bedrock forming a semi-continuous surface close to or exposed through the water surface.	Indicative of high energy, supply-limited transport conditions (Brierley and Fryirs, 2005)
Cascade	Area of highly disturbed water tumbling over and around disorganised boulders	Presence indicates supply-limited transport regime and strong influence of non-fluvial (e.g. hillslope, glacial, etc.) processes (Montgomery and Buffington, 1997)
Step	Flow falls near vertically over single channel-spanning line of large clasts causing disturbance to water surface.	Presence indicates supply-limited transport regime but greater influence of fluvial processes than cascade-dominated reaches (Montgomery and Buffington, 1997)
Rapids	Sequences of partially or fully channel-spanning, organised ribs with fewer exposed boulders than cascades but greater areal proportion of disturbed water surface than riffles	Presence indicative of transport-limited conditions but greater transport capacity than riffle-dominated reaches (Brierley and Fryirs, 2005)
Riffle	Area of disturbed water surface with negligible bed material exposure	Presence indicative of transport-limited conditions (Brierley and Fryirs, 2005)

1 *Table 2: Definitions of features identified and counted from Google Earth images.*

2

	PC1	PC2	PC3	PC4
BEFORE ROTATION				
Eigenvalue	4.209	2.709	1.524	1.157
Variability (%)	32.380	20.840	11.723	8.898
Cumulative %	32.380	53.221	64.944	73.841
AFTER ROTATION				
Variability (%)	31.199	15.638	11.491	15.513
Cumulative %	31.199	46.838	58.328	73.841
LOADINGS				
Active channel sinuosity	-0.596	0.589	-0.099	-0.201
Baseflow:Active channel sinuosity	**0.816**	0.392	-0.021	0.043
Active:Baseflow channel width	**0.827**	-0.112	0.145	0.169
Coefficient of variation of active channel width	*0.692*	-0.004	-0.215	0.199
Active lateral bars	**0.910**	-0.033	0.140	-0.053
Active mid-channel bars	**0.800**	-0.054	0.110	-0.125
Active point bars	0.098	**0.853**	0.048	-0.187
Channel cutoffs	0.006	**0.736**	-0.241	-0.138
Bedrock	-0.069	-0.017	**0.859**	0.259
Cascades	0.167	-0.284	0.071	**0.857**
Steps	0.211	-0.314	-0.085	**0.767**
Rapids	0.249	-0.224	**0.746**	-0.260
Riffles	0.504	-0.127	-0.138	*-0.614*

Table 3: Eigenvalues, percentage variability explained (before and after a varimax rotation), and variable loadings on the first four PCs of a Principal Components Analysis of channel dimension and physical feature variables. (Note that loadings > 0.7 are emboldened and loadings > 0.6 and <0.7 are in italics and underlined).

Variable	K	DF	p	Significant differences between classes	Bonferroni corrected significance level
PC1	123.8	4	<0.0001	C, E > A, D B > A	0.005
PC2	91.1	4	<0.0001	B > A, C, D, E A > C, E	0.005
PC3	75.3	4	<0.0001	D > A, B, C, E B, C, D > E	0.005
PC4	112.3	4	<0.0001	E > A, B, C A, B, D > C	0.005

Table 4: Results of Kruskal-Wallis tests (followed by multiple pairwise comparisons, based on Dunn's procedure with Bonferroni correction), applied to PC scores on each of the 5 clusters identified using agglomerative hierarchical clustering.

Class	PC1	PC2	PC3	PC4	Description	Example	Google Earth image
A	-				Laterally stable	Abhainn an t-Strath Chuileannach (UK)	
B	+	+			Active sinuous-meandering	Allier (France)	
C	+	-		-	Transitional (near-braided)	Feshie (UK)	
D			+	+	Bedrock	Ardèche (France)	
E	+	-	-	+	Cascade/step dominated	Bregenzer Ach (Austria)	

Table 5: Summary of the range (+ = positive, - = negative, blank = intermediate) of significantly different PC scores for reaches in each class in relation to each PC, and a brief description of each class based on interpretation of the environmental gradients described by each PC. (All images obtained from Google Earth. Additional copyright attributions: Allier - Image © 2018 CNES/Airbus, Image © 2018 DigitalGlobe; Feshie – Image © Getmapping plc; Abhainn an t-Strath Chuileannach – Image © 2018 Getmapping plc; Ardèche – Image © 2018 Google; Bregenzer Ach – Image © 2009 Geobasis-DE/BKG, Image © 2018 DigitalGlobe, Image © 2018 Google).

Class	PC1	PC2	PC3	PC4	Description	Example	Google Earth image
A	-				Laterally stable	Abhainn an t-Strath Chuileannach (UK)	
B	+	+			Active sinuous-meandering	Allier (France)	
C	+	-		-	Transitional (near-braided)	Feshie (UK)	
D			+	+	Bedrock	Ardèche (France)	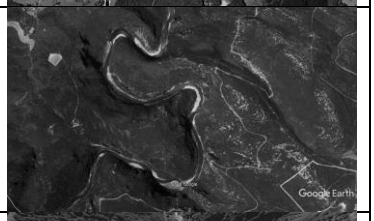
E	+	-	-	+	Cascade/step dominated	Bregenzer Ach (Austria)	

Table 5: ***GREYSCALE VERSION FOR PRINT VERSION*** *Summary of the range (+ = positive, - = negative, blank = intermediate) of significantly different PC scores for reaches in each class in relation to each PC, and a brief description of each class based on interpretation of the environmental gradients described by each PC. (All images obtained from Google Earth. Additional copyright attributions: Allier - Image © 2018 CNES/Airbus, Image © 2018 DigitalGlobe; Feshie – Image © Getmapping plc; Abhainn an t-Strath Chuileannach – Image © 2018 Getmapping plc; Ardèche – Image © 2018 Google; Bregenzer Ach – Image © 2009 Geobasis-DE/BKG, Image © 2018 DigitalGlobe, Image © 2018 Google).*